Stabilizing Electro-Optic Modulation Depth With Carrier to Sideband Ratio by Intermediate Optical Beatings

Jie Wang, Guochao Wang, Yaning Wang, Mei Hu, Xiao Yu, Mingyue Yang, Xu Zhang, Huankai Zhang, Aiai Jia, Lingxiao Zhu, Shuhua Yan, and Jun Yang

***Abstract*—Electro-optic modulation with a constant modulation depth plays important roles in quantum metrology, microwave photonics, and optical precision measurement and sensing, etc. To compensate the continuous drift of the half-wave voltage and maintain the modulation depth, we incidentally generated a reference laser to make intermedia optical beatings with the carrier and +1st sideband, and tightly locked the carrier to sideband ratio by extracting the relative microwave power of those intermedia beat signals using a home-made electronic control module. Experiments of the short-term test for locking bandwidth, the anti-jamming capability, and the long-term stability were demonstrated. As is verified that, the locking bandwidth was estimated up to tens of kHz, and the anti-jamming capability was confirmed despite of a strong hair-dryer agitation. The long-term stability for the modulation depth stabilization showed that the peak-to-peak relative stability for 150-minute was 5.67 $\times$ 10^{-6}, and the Allan deviation reached a minimum of 2.19 $\times$ 10^{-7} at an averaging time of 400 s, which is improved by more than four orders of magnitude compared with the open-loop regime. We believe the reported method as well as the designed module is versatile and potential to precision measurement and sensing applications badly requiring a stable modulation depth, such as atom interferometry, optical interferometry and lidar detection.**

***Index Terms*—Electro-optic modulator, modulation depth, carrier to sideband ratio, optical beating.**

Manuscript received August 30, 2021; revised October 10, 2021; accepted October 14, 2021. Date of publication October 19, 2021; date of current version November 2, 2021. This work was supported in part by China Postdoctoral Science Foundation under Grant 2020M683729, in part by Science Foundation of Hunan Provincial, China under Grant 2021JJ30774, in part by Young Elite Scientists Sponsorship Program by CAST 2018QNRC001, in part by the National Natural Science Foundation of China under Grant 12004428, and in part by Natural Science Foundation for outstanding young of Hunan Provincial China under Grant 2021JJ20047. *(Jie Wang and Guochao Wang contributed equally to this work.) (Corresponding authors: Guochao Wang; Shuhua Yan.)*

Jie Wang, Yaning Wang, Xiao Yu, Mingyue Yang, Xu Zhang, Huankai Zhang, Aiai Jia, Lingxiao Zhu, Shuhua Yan, and Jun Yang are with the College of Intelligence Science and Technology, National University of Defense Technology, Changsha 410073, China, and also with the Interdisciplinary Center for Quantum Information, National University of Defense Technology, Changsha 410073, China (e-mail: 1040314781@qq.com; wangyayaning@163.com; 18182111643@163.com; 2226132270@qq.com; sdzczx95@163.com; zhk18@163.com; jiaaiai1988@163.com; zhulingxiao31@163.com; yanshuhua996@163.com; john323@163.com).

Guochao Wang is with the College of Intelligence Science and Technology, National University of Defense Technology, Changsha 410073, China, with the Interdisciplinary Center for Quantum Information, National University of Defense Technology, Changsha 410073, China, and also with the High-tec Institute of Xi’an, Xi’an 710025, China (e-mail: wgc.19850414@163.com).

Mei Hu is with the Interdisciplinary Center for Quantum Information, National University of Defense Technology, Changsha 410073, China (e-mail: humei@nudt.edu.cn).

Digital Object Identifier 10.1109/JPHOT.2021.3120807

I. Introduction

ELECTRO-OPTIC modulators (EOMs) have a wide range of applications in the fields of quantum information technology [1]–[4], optical fiber communications and sensing [5]–[8], and microwave photonics [9]–[11], etc. Electro-optic modulation, such as phase modulation, applies an electric field to the crystal via electrodes for a phase offset of the optical carrier passing through that crystal, and sinusoidal modulation on the amplitude of that electric field results in generating a series of equally spaced sidebands centralized as the carrier in the optical frequency domain. The modulation depth, as an intuitive understanding of quantity and relative power on generated sidebands, is routinely relevant with the phase offset and physically determined by the half-wave voltage and the driving voltage. In general, if the driving voltage is measured and fixed, the modulation depth could be definite and constant. However, practically, the half-wave voltage is apt to temporally change with variations of factors, such as environmental temperature and input light polarization [7], [12]–[17], causing the modulation depth unstable. In many applications of EOM, the modulation depth is expected to be strictly constant. For instance, to eliminate AC-Stark shift of an atom interferometer, the modulation depth needs to be fixed at a specific value when making a Raman light pair by phase modulating [4], [18]. Furthermore, in a nanometer-resolution phase modulating interferometer where homodyne detection is implemented by phase generated carrier demodulation, the modulation depth needs to be well preserved for suppression on nonlinear distortion [8], [19]. Consequently, stabilizing the modulation depth of EOM is perfectly useful and necessary.

Apart from phase offset, the modulation depth also can be evaluated by the relative power of the carrier and sidebands with a Bessel expansion. Moreover, in a certain range of the modulation depth, the power ratio between the carrier and sidebands, called as carrier to sideband ratio (CSR), has a one-to-one correspondence with the modulation depth. Therefore, in that sense, the modulation depth can be stabilized by gaining and feedback controlling the CSR. A reported approach directly observed the power of the carrier and sidebands using a spectrometer, such as a Fabry-Perot interferometer (FPI), obtained the power ratio between the carrier and one sideband, and ultimately calibrated the CSR of phase modulated Raman lights [20]. However, that approach has a very slow update rate limited by the scanning time of FPI, and cannot achieve real- time and precise calibration of the CSR. An alternative method, proposed by L. Zhu [4], converted the optical CSR into microwave power ratio by beating the carrier and one sideband with a reference beam, and then the CSR was achieved and the modulation depth was locked by the feedback control of the modulation power using a radio frequency spectrum analyzer (RFSA). But the locking bandwidth is still low, no more than 10 Hz resulted from the acquisition time of RFSA, and thus that method is only suitable for static occasions without intense jam.

In this paper, we advance the intermedia beating method to build an electro-optic phase modulation module capable of stabilizing modulation depth with a high locking bandwidth being enlightened by the literature [4]. Instead of straight acquisition on RFSA, we dedicatedly extract the respective beating signals of the carrier and one sideband with a self-referenced laser by filtering intermediate beating signals from a highspeed detector, and the high updated CSR is acquired after RF power detection and division. This designed module is validated to realize low-drift, fast, and steady stabilization of the modulation depth, which is immune to disturbing factors such as the environmental mutation.

II. Principle and Setup

The CSR of an EOM fluctuates continuously over time, and it reflects the stability of the modulation depth. Therefore, extracting and locking the CSR can be implemented to stabilize the modulation depth. When a reference laser, whose optical frequency is located between the carrier and the +1st sideband, is used to couple with the modulated laser, two intermedia beatnotes are generated, one formed by the carrier and the reference laser, the other formed by the +1st sideband and the reference laser. Theoretically, the relative optical power ratio of the carrier and the +1st sideband is expected to be calculated by extracting the relative microwave power ratio of intermedia beatnotes. The nominal powers of two intermedia beating signals, P_0 and $P_{+1\mathrm{st}}$, detected by the photodetector are written as

$$\begin{cases} P_0 \propto \alpha_0 \cdot I_{ref} \cdot I_0 \\ P_{+1st} \propto \alpha_1 \cdot I_{ref} \cdot I_{+1st} \end{cases} \tag{1}$$

where α_0 is the detection efficiency for the beating signal between the reference beam and the carrier while α_1 is for the beating signal between the reference beam and the +1st sideband. I_0, $I_{+1\mathrm{st}}$ and I_{ref} are the intensities of the carrier, the +1st sideband, and the reference beam, respectively. Then, the relative optical power ratio γ_{CSR} for CSR is concluded as

$$\frac{P_0}{P_{+1st}} = \frac{\alpha_0 \cdot I_0}{\alpha_1 \cdot I_{+1st}} = \frac{\alpha_0}{\alpha_1} \cdot \gamma_{CSR} = \alpha \cdot \gamma_{CSR} \tag{2}$$

where α denotes α_0/α_1.

As we use the method of extracting the relative microwave power ratio of intermedia beatnotes to match the optical power ratio, in the actual process of microwave separation and power detection, the microwave powers ratio is distorted due to the unbalanced insertion loss of radio frequency line, the inconsistency of detection gain and filter gain, the detected microwave power ratio γ_{MP}, as well as microwave power signals MP_0 and $MP_{+1\mathrm{st}}$ on microwave power detectors for beatnotes (MPDB), is expressed as

$$\gamma_{MP} = \frac{MP_0}{MP_{+1st}} = \beta \frac{P_0}{P_{+1st}} = \beta \cdot \alpha \cdot \gamma_{CSR} \tag{3}$$

where β is the coefficient for the above unbalanced loss and inconsistency of microwave detection, while α for the coefficient of optical detection. Consequently, there is scaling factor $\beta\cdot\alpha$ between the targeted γ_{CSR} and the detected γ_{MP}, which is considered as a systematic error. Moreover, once the parameters of optics and electronics are confirmed, the systematic error is determined to be calibrated.

The schematic diagram of the experimental setup is shown in Fig. 1, the optical module shown in Fig. 1(a) while the electronic control module in Fig. 1(b). The input laser beam from a fiber laser (NKT Photonics, Koheras-BASIK-E15), is fiber-split into two beams. One is phase modulated by an EOM (iXblue, MPZ-LN-10) to generate the carrier and sidebands with the driving microwave source operated at 1.7GHz. The other one is 700MHz up-shifted by an acoustic-optic modulator (CETC, SGY350/350-1550P-D01), regarded as the reference beam. After respective modulations, the two beams are recombined to produce optical beating signals, which are converted into electrical signals by a photodetector (Menlo Systems, FPD310-FC-NIR) with a bandwidth of 1 MHz $\sim$ 1.5 GHz. The electrical signals are input into the electronic control module, which adaptively generates a microwave signal to act on the EOM for locking control. Finally, the servo loop is built and the modulation-depth-stabilized output beam is monitored by a Fabry-Perot interferometer (Thorlabs, SA210-12B) simultaneously.

Fig. 1(b) shows the electronic control module, the beating signals are split into two channels, which are respectively filtered by two bandpass filters (BPF) with center frequencies at 0.7 GHz and 1 GHz, and both filters have a bandwidth of 300 MHz versus an attenuation of 1dB. Therefore, the beating signals, at 0.7GHz representing the carrier and the 1GHz signal representing the +1st sideband, are extracted individually. Two identical microwave power detectors (Herotek, DZM185AA) are used to transform the beating signals into the voltage signals. After that, the power ratio γ_{MP}, corresponding to CSR, is obtained by a divider. By comparing the ratio with the reference voltage, an error signal is generated through the PI controller to tune the VCA (Mini-Circuits, ZX73-2500-S+), and the driving power of EOM is ready to change with the PI controller for stabilizing the modulation depth.

It is worth mentioning that we deliberately make a digital control way to flexibly change the modulation depth by adjusting the gain coefficient μ of the divider in the integrated electronic module. When the locking is on, the ratio synthetized on the divider is locked to the reference voltage, which is expressed as

$$V_{set} = \mu \frac{MP_0}{MP_{+1st}} = \mu \cdot \beta \cdot \alpha \cdot \gamma_{CSR} \tag{4}$$

where V_{set} is a settled and persistent voltage for the reference signal. According to Equation (4), due to the existence of the coefficient term, the actual power ratio γ_{CSR} can be calibrated as $V_{set}/(\mu\cdot\beta\cdot\alpha)$, and the locking point can be tuned by μ. Specially, when the coefficient μ is tuned to make $\mu\cdot\beta\cdot\alpha = 1$, the real γ_{CSR}

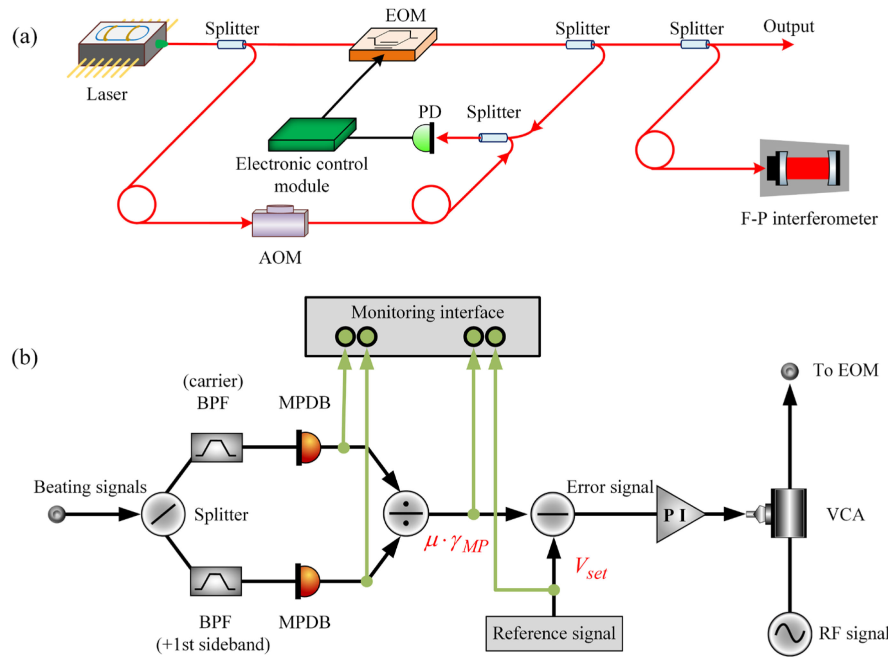

Fig. 1. Experimental setup. (a) Optical module. EOM, electro-optic modulator. AOM, acousto-optic modulator. (b) Electronic control module. BPF, band pass filter. MPDB, microwave power detectors for beatnotes. VCA, voltage-controlled attenuator.

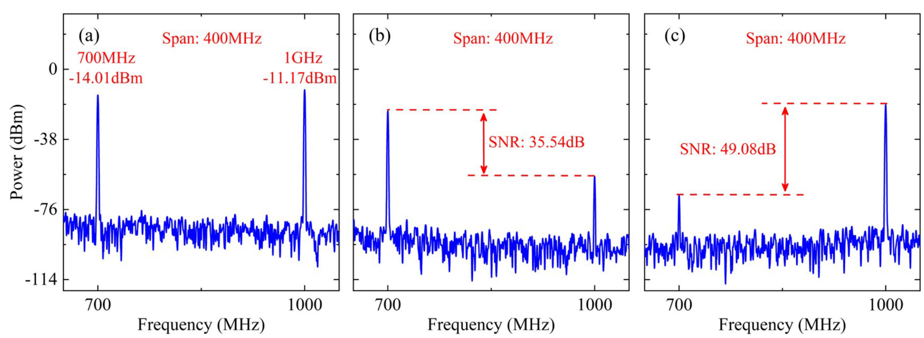

Fig. 2. The observed frequency spectrums of mixed beating signals by coupling the EOM beam and the reference beam (a), the filtered beating signal for the carrier (b), and the filtered beating signal for the +1st sideband (c).

for the exact modulation depth is directly equivalent to the fixed value of V_{set}.

III. Results and Discussions

After mixing the beam modulated by the EOM with the reference beam, the beating signals generated with the 18 dBm power driving the EOM were recorded by an RFSA (Anritsu, MS2830A). Fig. 2(a) shows the beating signals of 700 MHz and 1 GHz, representing the carrier and the +1st sideband, respectively. As is shown in Fig. 2(b) and Fig. 2(c), the beating signals are separately filtered by BPFs into individuals, and the signal to noise ratio (SNR) reaches 35.54 dB and 49.08 dB, respectively.

The filtered beating signals were converted into the voltage signals by MPDBs, and then γ_{MP} are extracted to realize the locking of the CSR with the controlling of servo loop. As analyzed above, there is a coefficient term $\beta\cdot\alpha$ between γ_{MP} and γ_{CSR}, this means that when γ_{MP} is well locked, γ_{CSR} may not be the same regime. Therefore, to be sure of that, MP_0, $MP_{+1\mathrm{st}}$, and γ_{MP} were monitored by MPDBs, while the optical carrier, +1st sideband, and CSR were simultaneously monitored by the FPI, as shown in Fig. 3. The above results were recorded by a digital oscilloscope (Tektronix, MSO64B) for a duration of 90 minutes with a sampling rate of 2.5 kHz. Among them, the results of carrier, +1st sideband were obtained by searching voltage peak for the scan results of FPI. when the servo loop is open, the fluctuations of γ_{MP} and CSR tend to be consistent, it could be explained that $\beta\cdot\alpha$ is considered as a fixed constant and has little effect on the fluctuation of CSR in the closed-loop regime. At the timescale of 46th minute, the servo loop is closed. The results of MPDBs show that the peak-to-peak (P-to-P) stability of γ_{MP} relative to the averaged value reaches 0.82%, while that of the open-loop regime is 16.33%. Moreover, the root-mean-square (RMS) stability of the γ_{MP} is 0.07%, while 4.10% for the open-loop regime. Simultaneously, the results of the FPI show that the P-to-P stability of CSR is improved from 19.03% to 3.99%, and the RMS stability is improved from 4.57% to 0.70%. Two monitoring methods verify that our module successfully suppresses the CSR fluctuations.

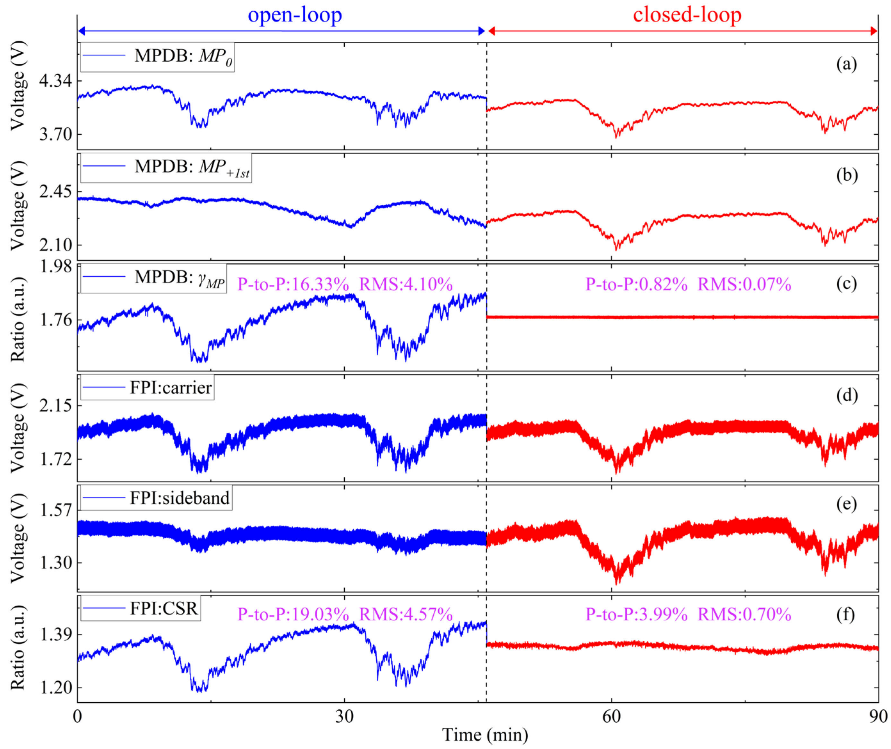

Fig. 3. The results of CSR stabilized for 90 minutes in the MP_0 (a), $MP_{+1\mathrm{st}}$ (b), and γ_{MP} (c) regimes obtained by microwave power detectors for beatnotes, and the optical carrier (d), +1st sideband (e) and CSR (f) regimes obtained by the Fabry-Perot interferometer at the same time. These results were recorded by a digital oscilloscope.

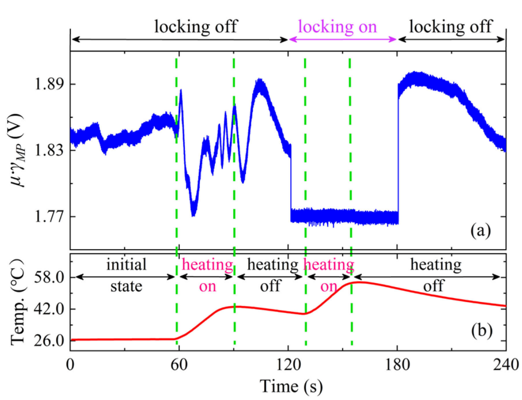

Fig. 4. The influence of temperature on the EOM in the open-loop and closed-loop regimes.

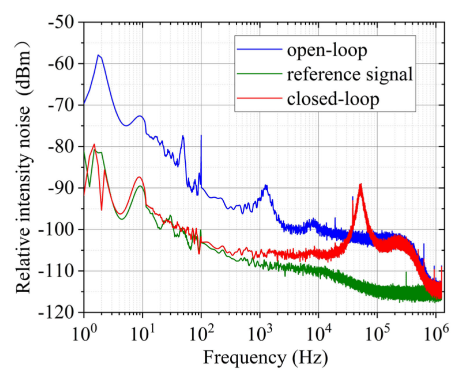

Fig. 5. The power spectrum of relative intensity noise. The blue and red curves represent the RIN in open-loop and closed-loop regimes, respectively. The green curves show the RIN of reference signal.

In addition, it can intuitively observe that MP_0 and $MP_{+1\mathrm{st}}$ vary synchronously as well as the carrier and +1st sideband. However, it can be seen that the fluctuations of CSR are larger than that of γ_{MP} in the closed-loop regime, and has roughly a same drift as the change of light intensity, it can be attributed to that the FPI is sensitive to light intensity noise

In order to prove the anti-disturbance ability of the module, we deliberately tested the influence and performance in front of temperature agitation on the EOM. The EOM with a temperature sensor probe (Thorlabs-TSP01) were closely enclosed in a sealing cover. A flow of strong hot air from a hair-dryer was blew into the sealing cover to heat the EOM. As shown in Fig. 4, the results of $\mu{\cdot}\gamma_{MP}$ direct from the divider were recorded on the digital oscilloscope (Tektronix, MSO64B) for a duration of 240 s with a sampling rate of 2.5 kHz. Basically, the whole duration is divided into several segments according to locking on or locking off as well as heating on or heating off. First, when the servo loop is open without temperature disturbance, deemed as the initial state, the $\mu{\cdot}\gamma_{MP}$ has a drift on its own. At the timescale of 60th second, the hair-dryer is turned on for 30 seconds to heat the EOM with a temperature increment of 16°C, bringing a violent oscillation on the value of $\mu{\cdot}\gamma_{MP}$ from 1.77V to 1.90V. As the hot air is cutoff, that oscillation becomes slow. At the timescale of 120th second, when the servo loop is closed, the locking for CSR is obviously achieved with suppressing the fluctuation within 0.018V. Despite of turning on the hair-dryer again at the

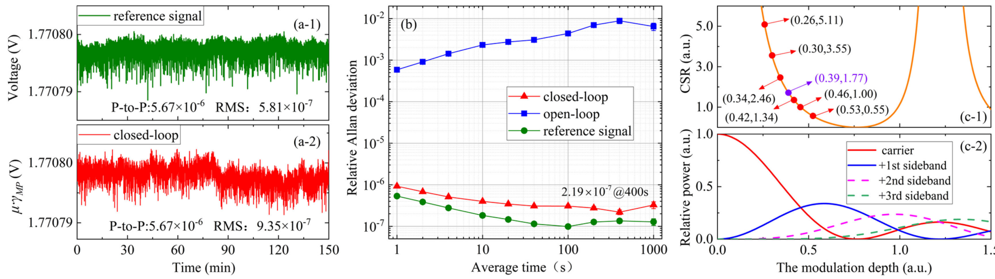

Fig. 6. (a) The result of CSR stabilized for 150 minutes recorded by a data logger. (b) The relative Allan deviation in the open-loop regime (blue squares) and closed-loop regime (red triangles). The green circles represent the relative Allan deviation of the reference signal. (c-1) Curves shows the theoretically calculated relationship between CSR and the modulation depth. (c-2) Curves describe the relative power in the carrier and first three-order sidebands for a normalized modulation depth from 0 to 1.5.

timescale of 128th second and for 30 seconds, the locking state and performance are well maintained even with temperature up to 55°C. Finally, when the loop is open again, the released $\mu{\cdot}\gamma_{MP}$ jumps and returns to the initial level gradually. The above results testify the anti-disturbance ability of the module.

A digital oscilloscope was used to sample the $\mu{\cdot}\gamma_{MP}$ for a duration of 4 s with a sampling rate of 2.5 MHz. With the fast Fourier transform (FFT), the power spectrum of relative intensity noise (RIN) was analyzed and shown in Fig. 5. When the servo loop is closed, the peak noise at the offset frequency of 1.75 Hz is suppressed by 26.6 dB compared to that of the open-loop regime, and reaches the level of -84.5 dBm. In the range of 1 Hz$\sim$10 kHz, the RIN of closed-loop is close to the reference signal noise, and reaches the level of -107.2 dBm at 10 kHz. Moreover, the bump, indicating the bandwidth of the whole controlling system, is visible at 52 kHz on the closed-loop RIN curves. We think this bump occurs due to the side effect of PI controlling, the height and position of which are to change when tuning the PI parameters.

In order to evaluate the long-term stability of locking CSR, γ_{CSR} and the reference signal were recorded for 150 minutes by a data logger (Keysight, 34461A), shown in Fig. 6(a). When the servo-loop is closed, γ_{CSR} is locked at the special point with the value of $\gamma_{CSR} = V_{set} = 1.77$ on basis of calibration, and the P-to-P stability of γ_{CSR} and the reference signal reaches 5.67×10^{-6}. Simultaneously, the RMS stability of γ_{CSR} is 9.35×10^{-7}, while that of the reference signal is 5.81×10^{-7}.

Fig. 6(b) shows the relative Allan deviations for the data of 150 minutes. In the closed-loop regime, the relative Allan deviation of γ_{CSR} at 1 s averaging time is improved by about three orders of magnitude from 5.87×10^{-4} to 9.25×10^{-7} than that of the open-loop regime. It is worth noting that a maximum noise suppression is obtained by about five orders at 400 s averaging time from 8.85×10^{-3} to 2.19×10^{-7}. Moreover, the γ_{CSR} at 1000 s averaging time reaches 3.27×10^{-7}, more than four orders of magnitude lower than open-loop regime.

As we have discussed that within a certain range, the modulation depth can be uniquely determined by CSR in the light of the Bessel expansion. For a clear view on the relationship of the modulation depth and CSR, Fig. 6(c-1) gives the simulated result of CSR versus the normalized modulation depth from 0 to 1.5 in an orange color, while Fig. 6(c-2) shows the relative power in the carrier and first three-order sidebands for the same modulation depth. As CSR approaches to infinity with the relative power of +1st sideband close to zero, the y-coordinate for CSR only appear from 0 to 6, which is obviously related to the modulation depth from 0.75 to 0.25 with one-to-one correspondence. Moreover, with that CSR maintaining at 1.77 in Fig. 6(a), the corresponding modulation depth is estimated to be stabilized at 0.39, and it is marked in the purple ball in Fig. 6(c-1). As the locking point of the modulation depth can be set by changing the coefficient of the divider, we have also achieved the feedback control of the modulation depth in other positions, as shown by the red balls in Fig. 6(c-1). Indeed, there is some dead zone for CSR locking, such as these points near the modulation depth of 0.75, the relative power for the carrier is so weak that a bad SNR will affect the control effect for locking CSR. However, when that modulation depth is demanded, we can make use of other sidebands with relatively higher power to stabilize the modulation depth. For example, the +1st sideband and the +2nd sideband are preferable to extract the power ratio for achieving the feedback control of the modulation depth near 0.75.

IV. Conclusion

We reported an electro-optic phase modulation module which stabilized the modulation depth by extracting the relative microwave power of intermedia beatings and locking the CSR. The locking bandwidth was estimated more than several tens of kHz by RIN analysis, and the anti-jamming capability was strongly verified through a hair-dryer agitation demonstration. Besides, the locking stability was also proved remarkable from the long-term measurement results of CSR. For 150-minute locking results, the peak-to-peak relative stability was about 5.67×10^{-6}, and the Allan deviation reached a minimum of 2.19×10^{-7} at an averaging time of 400s, improved by more than four orders of magnitude compared with the open-loop regime. The reported method, as well as the experimental module, has been validated to stabilize the modulation depth of EOM with high performance, which is versatile and competent to precision measurement and sensing that have strict requirement on a stable modulation depth.

References

[1] M. Kasevich, D. S. Weiss, E. Riis, K. Moler, S. Kasapi, and S. Chu, “Atomic velocity selection using stimulated Raman transitions,” *Phys. Rev. Lett.*, vol. 66, no. 18, pp. 2297–2300, 1991.

[2] K. F. Reim *et al.*, “Towards high-speed optical quantum memories,” *Nat. Photon.*, vol. 4, no. 4, pp. 218–221, 2010.

[3] L. Zhu *et al.*, “Application of optical single-sideband laser in Raman atom interferometry,” *Opt. Exp.*, vol. 26, no. 6, pp. 6542–6553, 2018.

[4] L. Zhu *et al.*, “Measurement and control of the sideband to carrier ratio of an electro-optic modulator used in atom interferometers,” *Opt. Exp.*, vol. 25, no. 10, pp. 11365–11376, 2017.

[5] A. Aray and S. G. Sabouri, “Plasmonic Bragg microcavity as an efficient electro-optic modulator,” *Opt. Exp.*, vol. 28, no. 14, pp. 20523–20531, 2020.

[6] R. Luo, H. Jiang, S. Rogers, H. Liang, Y. He, and Q. Lin, “On-chip second-harmonic generation and broadband parametric down conversion in a lithium niobate microresonator,” *Opt. Exp.*, vol. 25, no. 20, pp. 24531–24539, 2017.

[7] C. Wang, M. Zhang, B. Stern, M. Lipson, and M. Lončar, “Nanophotonic lithium niobate electro-optic modulators,” *Opt. Exp.*, vol. 26, no. 2, pp. 1547–1555, 2018.

[8] S. Zhang, B. Chen, L. Yan, and Z. Xu, “Real-time normalization and nonlinearity evaluation methods of the PGC-arctan demodulation in an EOM-based sinusoidal phase modulating interferometer,” *Opt. Exp.*, vol. 26, no. 2, pp. 605–616, 2018.

[9] C. A. Schuetz, J. Murakowski, G. J. Schneider, and D. W. Prather, “Radiometric millimeter-wave detection via optical upconversion and carrier suppression,” *IEEE Trans. Microw. Theory Techn.*, vol. 53, no. 5, pp. 1732–1738, May 2005.

[10] S. Zhang, H. Wang, X. Zou, Y. Zhang, R. Lu, and Y. Liu, “Calibration-free electrical spectrum analysis for microwave characterization of optical phase modulators using frequency- shifted heterodyning,” *IEEE Photon. J.*, vol. 6, no. 4, Aug. 2014, Art. no. 5501008.

[11] J. Zhou *et al.*, “Photonic measurement of microwave frequency based on phase modulation,” *Opt. Exp.*, vol. 17, no. 9, pp. 7217–7221, 2009.

[12] N. Jagatpal, A. J. Mercante, A. N. R. Ahmed, and D. W. Prather, “Thin film lithium niobate electro-optic modulator for 1064 nm wavelength,” *IEEE Photon. Technol. Lett.*, vol. 33, no. 5, pp. 271–274, Mar. 2021.

[13] D. H. Jundt, “Temperature-dependent Sellmeier equation for the index of refraction, n_e, in congruent lithium niobate,” *Opt. Lett.*, vol. 22, no. 20, pp. 1553–1555, 1997.

[14] A. Rao and S. Fathpour, “Compact lithium niobate electrooptic modulators,” *IEEE J. Sel. Topics Quantum Electron.*, vol. 24, no. 4, pp. 1–14, Jul./Aug. 2018.

[15] C. Shitong, C. Jianhua, and G. Wei, “A phase modulation method for improving the scale factor stability of fiber-optic gyroscope,” in *Proc. IEEE Int. Conf. Mechatronics Automat.*, May–Aug. 2008, pp. 37–42.

[16] P. Tang, D. J. Towner, A. L. Meier, and B. W. Wessels, “Low- voltage, polarization-insensitive, electro-optic modulator based on a polydomain barium titanate thin film,” *Appl. Phys. Lett.*, vol. 85, no. 20, pp. 4615–4617, 2004.

[17] D. Borlaug, P. T. S. DeVore, A. Rostami, O. Boyraz, and B. Jalali, “Demonstration of $V\pi$ reduction in electrooptic modulators using modulation instability,” *IEEE Photon. J.*, vol. 6, no. 5, 2014, Art. no. 6802409.

[18] Y. Wang *et al.*, “A new method for high-bandwidth servo control of the power ratio between two Raman beams for cold atom interferometer,” *Rev. Sci. Instrum.*, vol. 91, no. 10, 2020, Art. no. 103109.

[19] S. Zhang, Y. Chen, B. Chen, L. Yan, J. Xie, and Y. Lou, “A PGC-DCDM demodulation scheme insensitive to phase modulation depth and carrier phase delay in an EOM-based SPM interferometer,” *Opt. Commun.*, vol. 474, 2020, Art. no. 126183.

[20] L. Qin *et al.*, “A compact laser system for a portable atom interferometry gravimeter,” *Rev. Sci. Instruments*, vol. 90, no. 4, 2019, Art. no. 043104.